Effect of infrared light on protein behavior in contact with solid surfaces

Magdalena Kowacz[*] *and Piotr Warszyński*

Jerzy Haber Institute of Catalysis and Surface Chemistry Polish Academy of Sciences; Niezapominajek 8, PL-30239 Krakow

*****Corresponding author: nckowacz@cyf-kr.edu.pl

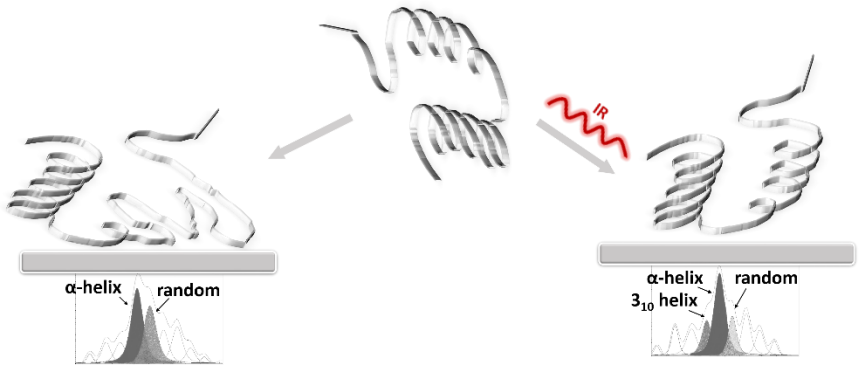

ABSTRACT. Adsorption of proteins at a solid surface affects characteristics of the surface (e.g. its biocompatibility) and functionality of the immobilized biomacromolecules. The latter is defined by the type of binding sites, protein conformation and its structural flexibility that enable functional motions to occur. Protein motions are only possible at certain level of hydration. Furthermore, water molecules act as lubricant facilitating sliding along solid surface. In this work we explore the potential of a remote physical trigger – a non-ionizing infrared radiation (IR) to affect protein-surface interactions. We report on IR-induced changes of hydrophilicity of the protein coatings on silica nanoparticles, impact of IR on monitored in-situ dynamic adsorption of proteins on silica surface and effect of IR on conformational state of adsorbed proteins. Our results indicate that IR can protect proteins from surface denaturation depending on the presence of strongly hydrated amino acid residues. Preservation of native fold results in protein coatings of higher hydrophilicity. IR can also facilitate displacement of surface active species that became adsorbed to protein apolar compartments and could otherwise promote denaturation. Apart from supporting native conformation, their removal increases protein-water interfacial tension and therefore promotes aggregation (hydrophobic attraction) of the protein-coated nanoparticles. By its ability to affect protein conformational state and interfacial characteristics (such as effective protein-water affinity) IR radiation can therefore modulate protein interactions.

KEYWORDS: protein adsorption, protein structure, protein corona, infrared radiation, protein-nanoparticle interaction

1. Introduction

Adsorption of proteins to nanoscale objects such as solid particles defines the effective properties of both, the solid and the adsorbed proteins forming particle's corona. Due to a large surface to mass ratio of nanoscale particles, mainly interfacial characteristics are responsible for their behavior in the environment. Therefore, the response of different systems, including biological ones, to protein-coated nanoparticles effectively depends on a soft protein corona with respect to its structure, dynamics and functionality [1-3].

Not only the interplay of particles with their environment but also mutual particle-particle interactions are determined by surface-adsorbed proteins. Thus, properties like colloidal stability of nanoparticle suspension or character of contacts on their close packing will in fact reflect surface-adsorbed protein-protein interactions at different separations (the characteristics important for bioengineering applications). Aggregation of nanoparticles in solution, determined by mutual attraction of protein coronas, may have important implications for their behavior as size of the aggregates will decide on their ability to cross biological barriers (like entering the cell).

It has been recognized that self-assembly of macroions with the overall net charge of the same sign, including biomacromolecules, is driven mainly by dipole-like interactions [4-10]. One possibility for emergence of effective dipoles results from heterogeneous patchy distribution of protein surface charges that generate short-range attractions overcoming long-range electrostatic repulsion between like-charged objects [9,10]. Alternatively, effective dipoles may be created by non-evenly distributed

counterion clouds [4-6,8], eventually structurally linked with surface charges by organized water bridges [7,11,12]. The larger the separation of surface charges from their counterions, provided by structured hydration layer, the larger effective dipole moment. The latter mechanism should be especially important for sterically restricted surface-adsorbed proteins, where the electrostatically incompatible patches of the same charge will remain exposed to the solvent while surface-adsorbed patches of the opposite sign will be shielded from the interaction.

It was shown by molecular simulations that in case of proteins freely diffusing in solution, the process of specific self-assembly could be assisted by adhesive hydrogen-bonded networks of water molecules that link protein interfaces from early intermediates to specific complex formation. [13]. This water mediation is recognized to increase gradually on transition to associated state and thus provide favorable thermodynamic gradient toward the self-assembled conformation. The existence of prolonged dynamic chains of H-bonded water molecules connecting amino acids of adjacent protein molecules is also recognized to exist in crystal lattices and to be necessary for their integrity [14]. On the other hand, the increased stability of hydrophilic nanoparticles in the high salt conditions were observed due to “hydration repulsion” [15].

Terahertz spectroscopy studies have revealed that dynamic hydration shell around proteins can extend to more than 15 Å, which corresponds to at least five layers of water molecules [16]. At the same time, the ability of proteins to induce structuring of their interfacial water layer has been revealed to play crucial role in protein biological functions [17-20]. An in-depth analysis of recent advances and current understanding of protein-water interplay can be found in a review of Bellissent-Funel at al [21].

Recent findings showed that infrared (IR) radiation can promote structuring of water molecules (effective hydration shell expansion) near hydrophilic interfaces [22] including protein interfacial water [23]. This IR-enhanced hydration was shown to be able to induce attractive interactions between like-charged colloids and biomacromolecules in solution [23,24]. These phenomena were explained by considering water-mediated charge separation (polarization/dipole formation).

In this work we explore the effect of IR light on i) protein-surface interactions that determine formation and functionality of the protein coronas and on ii) mutual interaction of particles coated by protein coronas.

2. Materials and Methods

2.1. Materials

Proteins, lysozyme (Lys) from chicken egg white (62791, Sigma-Aldrich), albumin (ovalbumin, OVA) from chicken egg white (A5503, Sigma) and bovine serum albumin (BSA)(A2153, Sigma) were used in this work. Stock solutions of proteins of concentration of 40 mg/ml were prepared in either Milli-Q water, 20 mM NaCl or in 20 mM imidazole buffer of pH = 7.36 and stored refrigerated at 4˚C before use.

Silicon dioxide SiO_2 nanoparticles (637238 Aldrich) of the average diameter of 10 nm – 20 nm were used to probe effect of adsorbed proteins on particle-particle interactions. Quartz crystal sensors (5 MHz quartz crystal QS-QSX303 from Biolin Scientific) were used to monitor in situ protein-surface interactions.

2.2. Sediment Volume Method

The sediment volume method was employed in this work to determine relative hydrophilicity of the sediment-forming particles according to the concept proposed by Vargha-Butler et al. [25]. In the frame of this theory the propensity of solid particles to either aggregate in solution (and form compact sediment) or stay apart (and create loose sediment) expresses relative affinity of the solid to the solvent and may be used to determine its hydrophilic/hydrophobic character. The more hydrophilic particles the less compact sediment they will form in an aqueous solution (as used in this work). That is due to increasing adhesion forces between solid and polar liquid with respect to the cohesion forces between particles.

For the sedimentation experiments, 250 μl of protein solution of lysozyme, ovalbumin or bovine serum albumin (40 mg/ml) was placed in a 1.5 ml Eppendorf tube and 500 μl of respective solvent (water, 20 mM NaCl or 20 mM imidazole buffer of pH = 7.36) was subsequently added. Then tube content was transferred to a plastic cuvette containing 25 mg of dry SiO_2 nanoparticles (10-20 nm in diameter) and 250 μl of the solvent was added to give final volume of 1000 μl and protein concentration of 10 mg/ml. Cuvette content was closed with a cap, gently mixed and stored in a vertical position for 72 hours. After sedimentation has taken place, sediment volume was measured by means of processing digital images of the cuvettes with the use of the program IC Measure [26]. In order to assure that sediment hydrophilicity is not affected by freely diffusing proteins present in solution, we have been exchanging the solution over the sediment with solvent only and observed no changes in sediment volume.

To examine the effect of infrared (IR) radiation on hydrophilicity of the protein-coated solid particles, the 250 μl of protein solution (40 mg/ml) was initially irradiated

for 10 min with the use of the Light Emitting Diode (LED) with the emission maximum in the IR range at wavelength λ = 2900 nm (LED29, Roithner-Lasertechnik) and the full width at half maximum of 350 nm. After the irradiation all the procedure was performed in exactly the same manner as in control experiments. For the irradiation step, LED was placed about 1.5 cm distance over the surface of protein solution and was operated by D-31M driver (Roithner-Lasertechnik) in a quasi-continuous wave mode (the mode of maximum average optical power from the LED) at 2 kHz and 200 mA. The emitted IR light represents a non-ionizing electromagnetic radiation (strongly absorbed by liquid water) and its maximum optical power ranges to 29.47 mW. The IR light of this particular wavelength was shown to have prominent effect on interfacial water [27], including protein hydration shell, and on protein-protein interactions. [23] In our previous work [23] we have been monitoring possible LED-induced temperature changes for the same time of exposure for 10 μl water drops. Temperature changes were negligible thus excluding bulk thermal effects of IR.

2.3. Quartz Crystal Microbalance

A Quartz Crystal Microbalance with Dissipation, QCM-D (the Q –Sense E4, Biolin Scientific) was used to monitor in-situ frequency and energy dissipation changes on adsorption of protein at silica (SiO_2) surface. For this purpose, a SiO_2 sensor (5 MHz quartz crystal QS-QSX303 from Biolin Scientific) was used as a substrate and protein solutions of either lysozyme (Lys), bovine serum albumin (BSA) or ovalbumin (OVA) of concentration of 1mg/ml (prepared in Milli-Q water or imidazole buffer of pH = 7.36) were used as analytes in contact with the sensor. SiO_2 sensors were cleaned in Piranha solution (a mixture of sulphuric acid (H_2SO_4) and hydrogen peroxide (H_2O_2) in 4:1

volume ratio) immediately before use. The baseline was calibrated with the respective solvent (water or buffer). After the frequency and energy dissipation levels become stable, the protein solutions were injected simultaneously to QCM-D cells with the use of a peristaltic pump at flow rate of 100 μl/min (corresponding to the laminar flow regime) [28]. After monitoring the adsorption, protein solutions were exchanged by respective solvent and sensors were washed to inspect for possible desorption of the loosely bound protein molecules and (as it emerged in our experiments) for additional solvent adsorption by surface immobilized proteins. At this washing step, in unbuffered conditions, exchanging protein solution by pure water is related with change of ionic strength and of pH (pH of Milli-Q water differs from pH of the unbuffered protein solution).

According to the Sauerbrey model [29], for a low dissipation system (relatively rigid adsorbed film of $\Delta D/\Delta f < 10^{-6}/10$ Hz where ΔD is the dissipation change and Δf the frequency change), the frequency decrease is linearly proportional to the adsorbed mass (Δm) per unit area, $\Delta m = - C \Delta fn/n$ (where C is the mass sensitivity constant C = 17.7 $ng/cm^2\ Hz^{-1}$ for a 5MHz crystal and n is the overtone number). In this context QCM acts as a very sensitive balance allowing for the in-situ monitoring of adsorption/desorption process at a molecular level. Additionally, dissipation changes are indicative of viscoelastic properties of the system with increasing dissipation meaning increasing softness of the adsorbed film.

To monitor possible changes in protein-surface interactions induced by IR radiation, protein solutions were exposed to IR before contacting them with the sensor. This was achieved by placing the LED (LED29, Roithner-Lasertechnik) immediately

over the wall of the inlet tube supplying the protein solution to the QCM-D cell (1 mg/ml at flow rate of 100 μl/min). LED was placed at a distance of about 15 cm from the tube entrance to the temperature controlled QCM-D chamber to allow for temperature equilibration before contact of the solution with the surface. LED29 was operated at 2 kHz and 200 mA (as in sedimentation volume experiments). During the final washing step the LED was switched off. In order to control if IR light could have some effects on frequency or dissipation response of the sensor in protein-free system, the control experiments were performed with water exposed to IR radiation in the same manner as in the case of protein solutions (baseline remained stable in this case). Additional experiments were also performed with proteins at different flow rates to still exclude possible heating effects at low flow regime (no differences in response of protein-surface interactions to IR at these different flows could be observed).

2.4. Fourier Transform Infrared - Attenuated Total Reflection (FTIR-ATR) spectroscopy

Infrared spectra of bovine serum albumin (BSA), albumin from chicken egg white (OVA) and lysozyme (Lys) from chicken egg white were recorded with the use of Thermo Scientific Nicolet iS10 FTIR Spectrometer equipped with Specac 25 Reflection Variable Angle ATR accessory and germanium crystal or with ConcentratIR2 accessory and 10 reflection diamond crystal. Data were accumulated over spectral range of 4000 cm^{-1}- 600 cm^{-1} with a nominal resolution of 4 cm-1 and 256 scans. Spectra of protein solution (20mg/ml or 40 mg/ml of protein) were recorded in water (without background electrolyte), in 20 mM NaCl and in 20 mM imidazole buffer of pH = 7.36. Spectra were recorded at control conditions and after exposure of solution of BSA, OVA and Lys to

infrared light (500 µl, 10 min. of irradiation). Irradiation was performed in the same manner as described in previous sections. In order to get insight into the conformation state of the adsorbed proteins, after the protein solution has been deposited on the ATR crystal surface it was left there for 10 min. in order to allow for adsorption of a protein layer from solution. Afterwards, protein solution was gently removed, crystal surface was rinsed several times with respective solvent (water, salt or buffer) and solvent was replaced over the adsorbed protein layer. Subsequently, spectra of adsorbed protein layer have been recorded in the same manner as spectra of dissolved proteins. In order to check if quickly developing adsorption layer has some impact on the spectra of dissolved proteins, after first scan of protein solution was acquired, crystal surface was rinsed several times with respective solvent and additional spectra has been measured after solvent replacement. Then those spectra of solvent with this adsorbed layer has been used as a background for subsequent measurements of dissolved proteins. The need to account for the adsorbed layer for accurate protein structure determination has been suggested by Goldberg and Chaffotte [30]. Apart from this additional measures, as a routine procedure ATR crystal surface was cleaned with gentle surfactant before each measurement. Therefore careful control was taken in order to avoid any bias that could come from the proteins adsorbed to the crystal surface.

Analysis of the secondary structure of the protein was carried out based on Fourier self-deconvoluted spectra in amide I region (1700 – 1600 cm-1) according to the procedure described in a protocol of Yang et al. [31]. Position of the peaks in deconvoluted spectra was adjusted in accord with the second derivative of the original spectra.

2.5. Colloidal characteristics. Zeta potential and size of the aggregates

In order to get some insight into the process of protein adsorption on silica nanoparticles and their effect on particle-particle interaction in solution we were measuring zeta potential (ZP) and size of aggregates (the hydrodynamic radius) of protein-decorated nanoparticles in solution. Both parameters were monitored by dynamic light scattering with the use of ZetaSizer Nano (from Malvern Instruments). For this purpose, nanoparticle suspensions were characterized either directly after their preparation (mixing IR-exposed or control protein solution with SiO_2 powder, as described in sediment volume experiments) or after 24 h or 72 h of the sedimentation process, where particles suspended over the sediment were measured. To validate if the measured ZP came from particles only and was not affected by freely diffusing proteins, we exchanged the solution over the sediment by pure water and subsequently measured values for resuspended solid (no differences were observed). For ZP and hydrodynamic radius of the aggregates additional experiments were performed with different protein concentrations of irradiated solutions (keeping the same final concentration as in sedimentation volume experiments), varying SiO_2 concentrations and with SiO_2 particles of different sizes (1-5 μm and 5-15 nm). These data are not reported in the present work but they confirmed trends that are described here for the selected system. We have also monitored pH of the protein solutions prepared in Milli-Q water without supporting electrolyte. The pH measurements were performed for protein concentration of 1mg/ml at room temperature.

3. Results and Discussion

3.1. Particle cohesion behavior

We have observed differences in sediment volume of the protein-coated nanoparticles depending on the composition of the protein corona, environmental conditions (water, 20 mM NaCl or buffer) and exposure to the electromagnetic radiation (IR). Presented in Fig. 1 differences of sediment volume of protein coated silica reflect the effect of an environment on the structure of particular protein-silica aggregates and their interfacial characteristics such as relative water affinity [25].

The results presented in Fig. 1. should be interpreted in conjunction with the characteristics of both individual proteins and protein-silica particles assemblies in solutions as reported in Table 1 and Fig. 2. Specifically, zeta potential (ZP) provides information about the net surface charge and resulting electrostatic interactions (Table 1). ZP of nanoparticles changes to highly positive on Lys adsorption and its magnitude resembles that of respective proteins for OVA and BSA coatings. Sensitivity of ZP of the protein-particle assemblies to the environment ionic strength, as opposed to uncoated SiO_2, further indicate that these are protein coronas that determine overall charge of the aggregates what further implies at least monolayer coating. Yet, for Lys the local environment of the nanoparticles [32] seems to support protein positive charging. As a consequence, ZP of the Lys coating, unlike ZP of dissolved protein, does not decrease on changing pH from salt to buffer (at which conditions Lys is less protonated). It might be due to higher near-surface concentration of positive ions compensating for SiO_2 negative charge. [33] Tendency of the system components to associate in solution (Fig. 2), considered in the light of electrostatic forces, points towards necessity to take into account local charges and their patchy distribution. Moreover, packing density of the

sediment confronted with the tendency of its components to aggregate in solution suggests the role of short-range hydration forces in defining sediment properties.

Table 1. Protein isoelectric point (pI), hydrodynamic radius (r) by DLS, molecular dimensions (mol. dim.), surface hydrophobicity (as binding constant of hydrophobic probe) and pH of unbuffered protein solutions. Zeta potential (ZP) of proteins, SiO_2 nanoparticles and protein-coated nanoparticles in different environments

	pI[a]	r (nm)	mol. dim. (nm)	Surface hydroph. K (M^{-1})[b]	pH[c]	ZP particles (mV)			ZP (mV)
					H_2O		NaCl (20mM)	buffer (20mM; pH = 7.36)	
Lys	11	2.5	3 x 3 x 4.5	7.69×10^4	4.03	24.1	13.2	13.0	3.65
OVA	4.5	3.6	7 x 3.6 x 3	7.57×10^5	7.58	-27.2	-21.2	-19.6	-22.2
BSA	4.8	4.0	4 x 4 x 14	8.20×10^5	7.63	-33.9	-24.4	-22.2	-20.9
SiO_2						-30.8	-30.4	-28.6	

a – from Aravind et al. [34]; b –from Cardamone and Puri [35]; c - pH values differing from protein pI result from the presence in protein samples counterions other than only H^+ and OH^- [36]

It has been recognized that in solution these are dipole-like rather than hydrophobic interactions that drive protein aggregation and lead to their colloidal instability [9,10,37]. Thus, in our case, interactions between negatively charged silica cores and solvent exposed positive patches of the protein shells can determine particle bridging and formation of aggregates. In this context, OVA has the lowest amount of positively charged amino-acid residues [38] and significant part of them can be engaged in forming direct contacts with negatively charged silica surface thus being shield from

the solvent. Therefore dipole-like interparticle attraction is least effective in the latter case and the most effective for particles decorated with Lys with its net positive surface charge, in which case the largest protein-silica aggregates are formed (Fig. 2).

For Lys as surface-adsorbed protein sediment has the largest volume in water (Fig. 1) due to the highest net positive surface charge of the protein that supports formation of large heteroaggregates with negatively charged silica particles. Charged residues interact also with water dipoles rendering additional hydrophilicity to the protein coronas and making sediment more swelled. Sediment volume of Lys-coated nanoparticles decreases on addition of salt, where the former is most compact. The effect of salt can be ascribed to screening by background electrolyte of protein surface charges. The latter is reflected in ZP of the protein-coated particles (Table 1) diminishing with increasing ionic strength. Screening reduces dipole-based particle bridging and results also in effective shirking of hydration layer.

For BSA and OVA, on the other hand, sediment volume increases on addition of salt and even further in the presence of a buffer. Presence of salt ions results in screening of protein surface charges. Because both proteins and the surface are negatively charged, screening reduces mutual repulsion. Furthermore, sodium cation exhibits higher propensity to bind to the amino acid residues of proteins than does chloride [39]. Consequently, also slight shift in favour of interactions promoted by positively charged residues can be expected on addition of NaCl. In a buffer with pH slightly lower from that of water and salt solution, BSA and OVA possess less negative surfaces what is expressed in ZP of protein-coated nanoparticles diminishing on changing the environment from water to salt and then to buffer (Table 1). Basic amino acid residues,

on the other hand, become slightly more protonated at lower pH what further supports dipole-like particle-protein attractions and formation of larger aggregates.

Apart from electrostatic interactions, presence of background ions affects also protein-water affinity. It has been recognized that weakly hydrated or polarizable ions exert propensity to non-polar protein compartments similarly to their behaviour at the air/water interface [40-43]. And chloride anion specifically, apart from binding to positively charged amino acid residues, thus screening surface charges, was shown to weakly associate with protein non-polar patches [44]. As adsorbed ions remain partially hydrated, they promote reduced protein-water interfacial tension and increase protein solubility [45-49]. Therefore, for the proteins with significant hydrophobic surface area (Table 1), addition of salt results also in increased protein-water affinity, causing sediment to be more loose (Fig. 1). Even exchanging of simple monovalent salts from KCl to NaCl at low concentration (0.001 M) induces non-negligible changes in protein zeta potential. [50] NaCl in particular has been shown to associate with surface of BSA and shift its isoelectric point. [50] Thus, the nature of the salt ions affects protein surface charge therefore modulating protein interaction with water dipoles. And it is recognized that addition of salts at low concentration induces protein salting-in, meaning its increased affinity for water. [51] The same mechanism operates even more effectively in buffered solution, where adsorption of surface active compound - an imidazole, which has been recognized to partition to hydrophobic interfaces [52, 53], renders protein more hydrophilic. This contributes to the increase of sediment volume especially for BSA and OVA with significant solvent exposed hydrophobic surface area [35,54], Table 1. For Lys the effect of lower net positive surface charge in buffer solution with pH closer to protein

isoelectric point is effectively attenuated by this added hydrophilicity. Thus sediment volume is only slightly reduced on changing environment from water to buffer.

Presented in Fig. 3 IR-induced macroscopic changes in sediment volume of the protein-coated silica nanoparticles reflect response of the proteins forming particle corona to IR light. Positive values on the Fig. 3 designate increase, while negative values reduction in sediment volume. Non-ionizing IR radiation is a physical trigger and does not affect chemical parameters of the solutions. Effect of IR-light can therefore result either from modification of protein interfacial characteristics, e.g. defined by surface adsorbed ions, and/or from different structural conformation of IR-exposed proteins (at constant pH and chemical composition). For Lys an increase of sediment volume was observed regardless of the environment. As the IR-induced enhancement of protein hydration has been evidenced previously by FTIR spectroscopy for irradiated lysozyme, myoglobin and haemoglobin in water [23], that increase can be attributed to the swelling of particle-protein network due to enhanced water affinity. For BSA the sediment volume increases in water and NaCl solution, due to enhanced hydration as mentioned above, whereas its large decrease (c.a. 20%) can be noted in the imidazole buffer. For OVA, IR-induced changes are least expressed and tend to promote more compact packing of the respective particles. The plausible explanation for both, enhanced hydration and apparent increase in protein-protein or protein-surface vs. protein-solvent affinity will be discussed further on.

3.2. Protein – surface interaction

The trends in protein partitioning to the solid surface on changing interaction environment from water to buffer are illustrated in Fig. 4 and 5. They can be qualitatively

justified by considering respective differences in protein interactions with silica surface depending on protein charge and hydrophilicity with the mass of adsorbed protein calculated based on the Sauerbrey model. Lys is more positively charged in pure water than in a buffer, therefore in the former case the final coverage of 64 ng/cm^2 was much lower than in a buffer (185 ng/cm^2). This is mainly result of electrostatic lateral repulsion. The final coverage for BSA was 69 ng/cm^2 in water and 47 ng/cm^2 in buffer, whereas for OVA the equilibrium coverage was 48 ng/cm^2 and 43 ng/cm^2 in respective environments. In both conditions the net electric charge of BSA and OVA is negative (as is the charge of a silica surface [55]), therefore, the adsorption occurs due to the presence of positive charges provided by protonated amino acid residues and hydrophobic protein domains [56]. As both proteins have in a buffered solution lower net surface charge (thus experience less mutual and surface repulsion) and more protonated amino acid residues, electrostatic interactions should promote increased protein adsorption. Nevertheless, the observed trends are just opposite suggesting prevalence of hydrophobic component. Thus, it is increase in water affinity of protein apolar compartments, due to adsorption of surface-active species, that attenuates their mutual attraction - the interaction that would promote denser packing, and reduces their propensity to partition to the solid. Such considerations are in agreement with previous studies showing that mainly charged arginine provides binding sites on protein adsorption to silica nanoparticles [57] with character of those specific contacts being possibly determinative for protein functionality [58]. Yet, for patchy molecules with polar and non-polar regions it is their hydration state that defines net surface coverage developed on the solid [59]. Thus large protein-particle assemblies can be formed in solution due to dipole-like many-body interactions within

this network, while packing density of individual protein coronas can be limited by short-range hydration repulsion between immobilized proteins [15].

A remarkable difference between observed adsorption kinetics in water and imidazole buffer is the presence of short lasting minima of the frequency of QCM crystal, i.e., maxima of the adsorbed mass (Fig.6). Those maxima can be attributed to the structural changes and the release of hydration water upon contact of protein with solid surface [60]. The depths of those maxima are enhanced by IR irradiation, which supports the observation on the effect of IR on protein hydration [23] and the results reported in Fig. 3. On the other hand, the effect of IR on the final coverage seems to be rather minor. After irradiation Lys coverage changes from 64 ng/cm^2 (no IR) to 55 ng/cm^2 (IR). For BSA irradiation reduces its adsorption from 69 ng/cm^2 (no IR) to 65 ng/cm^2 (IR). Only for OVA its propensity to the surface slightly increases on IR-exposure and changes from 48 ng/cm^2 (no IR) and 56 ng/cm^2 (IR) (experimental error ± 5 ng/cm^2). Comparison with respective sediment volumes (demonstrating persistent effect of hydration enhancement, Fig. 3) suggests that hydration water is effectively entrapped on participating in dipole-like interactions within protein-particle network.

For the adsorption of investigated proteins in imidazole buffer no initial minima were observed. This may indicate stabilization of hydration layer by imidazole ions. At those conditions much more significant differences in final mass (with exception of OVA) could be noted, i.e., 185 ng/cm^2 (no IR) vs. 131 ng/cm^2 for Lys and 47 ng/cm^2 (no IR) to 87 ng/cm^2 (IR) for BSA. The trends can be understood by considering that, in line with sediment volume experiments (Fig. 3), IR light increases hydration of Lys in a buffer what makes the adsorption layer more spongy (and the sediment more loose),

while it decreases hydration of more hydrophobic BSA and OVA making the protein layer (and the sediment) more compact.

3.3. IR protection from surface denaturation

To elucidate possible changes in the secondary structure of proteins adsorbed in various environments we inspect the IR spectra of proteins in solution and adsorbed at the surface of ATR crystal. Protein structural state in solution differs slightly depending on the chemical environment. In the case of BSA the degree of protein folding (defined by contribution of helical conformation) increases in the expected order from water through salt to buffer (Fig. 7 a, d and Fig. 8 a) and Table 2. All studied proteins undergo partial denaturation on the adsorption process as evidenced by the increase of the ratio of random coils.

Analysis of the infrared spectra of the surface-deposited proteins revealed that IR light prevents BSA (Fig. 7 c and 8 f) and Lys (Fig. 9 c) from denaturation on the process of adsorption to the solid surface but it has no effect for OVA (Fig. 9 f). Inspection of the spectra showed that 3_{10} helix was the conformational motif most liable for structure loss upon adsorption. In fact 3_{10} helix (usually located at the C-terminal of an α helix) is recognized to be much less stable than α helical conformation and structural transitions between these two have been evidenced [62-64]. Our data indicate that surface denaturation process can proceed by unfolding of α helixes through 3_{10} helix and β-turn intermediates to random coils (as evidenced by changes in the secondary structure of BSA and Lys, Fig. 7, 8 and 9) or by transition of 3_{10} helix to β sheet conformation in case of OVA (Fig. 9), what is in agreement with previously postulated mechanisms [62-66]. Another feature of infrared spectra associated with structural changes during the

Table 2. Percentage distributions of secondary structures of BSA, Lys and OVA in different environments in dissolved, adsorbed state and adsorbed state after IR-exposure. Please note that for irradiated BSA and OVA unfolding on adsorption process is hampered at the stage of α helix to 310 helix transition and does not proceed further to random coil (as in case of proteins adsorbed from non-irradiated solution). *(There are studies indicating that for BSA structures lying in the spectral region usually ascribed to β sheets correspond in fact to short-segment chains connecting α helical segments [61])

protein	envvir.	status	Secondary structure (%)				
			α helix	3_{10} helix	β - sheet*	β - turn	random
BSA	H_2O	dissolved	36	7	26	11	20
		ads.	29	-	34	14	23
		IR - ads.	28	13	29	17	12
	NaCl	dissolved	40	6	23	15	16
		ads.	27	-	32	17	24
		IR - ads.	34	10	29	17	10
	Imidazol buffer	dissolved	46	5	24	13	12
		ads.	30	-	32	14	24
		IR - ads.	33	12	26	17	12
Lys		dissolved	36	10	27	15	12
		ads.	33	-	29	20	18
		IR - ads.	33	9	23	17	17
OVA		dissolved	19	14	41	11	11
		ads.	20	-	52	17	10
		IR – ads.	20	-	47	21	12

adsorption process is shift to higher wavenumber of the band corresponding to α helixes (prevented by IR). The shift suggests lower polarization of C=O bonds (main components of the amide I band) and is consistent with weakening of hydrogen bonding of carboxylic groups that is necessary to maintain ordered conformation.

For BSA and Lys, IR light is apparently able to prevent helix from unfolding in contact with the solid surface. More folded conformation of proteins deposited from the irradiated solution can account for increased hydrophilicity of the corresponding protein

coronas (as random coils, which content increases on unfolding, have the largest solvent exposed hydrophobic surface area [67]). This further explains observations of less compact sediment (Fig. 3 for Lys and BSA, except in buffered conditions for the latter) and reduced tendency to adsorb in irradiated systems (Fig. 4 a and b and 5 a).The extent of the protection of the secondary structure seems to correlate with the presence of the positively charged basic amino-acid residues that have been recognized to hold water most strongly and create the longest-lived H-bonds with water [68]. The net amount of those residues, namely lysine, histidine and arginine is almost the same for Lys and BSA and the lowest for OVA [38] with the latter does not experiencing IR protection from surface denaturation. The correlation between the protective effect of IR, interfacial water structuring and presence of the strongly water-holding residues was demonstrated by results of our previous study [23]. That study indicated that IR-induced increase in cooperativeness and strength of H-bonds of protein interfacial water correlated with the protonation state of the basic amino-acid residues and that enhanced structuring of the hydration shell (acting as lubricant [69,70]) protected proteins from non-specific aggregation in solution. In this context it is interesting to consider different structural response of BSA and OVA to IR light (Fig. 8 and 9). Previous studies implied that BSA possess positively charged functional groups (mainly arginine) near hydrophobic compartments, while OVA has negatively charged groups near hydrophobic surface patches [54]. It is justified to expect that solvent-exposed hydrophobic regions of proteins will be preferentially excluded from solution and located in contact with the surface on the adsorption process. Thus, in case of BSA enhanced hydration of the adjacent positively charged amino acid residues can probably hinder further unfolding initiated by

spreading of the hydrophobic compartments at the solid surface. For OVA strongly water-holding residues are located away from the hydrophobic patches. Therefore increased hydration of the former does not prevent denaturation from proceeding. Further to this end, lysine, histidine and arginine are also the most amphiphilic among all amino acid residues [71] with lysine in particular having the largest hydrophobic solvent exposed surface area [72]. Then they by themselves may be prone to partition to the solid and enhanced hydration can attenuate this propensity.

3.4. IR-induced displacement of surface adsorbed ions

The structure change itself does not explain different adsorption behaviour of BSA (Fig. 4 and 5) or sediment structure of BSA-coated nanoparticles depending on the environment or slightly enhanced cohesion of particles decorated by OVA after irradiation. (Fig. 3). In the presence of imidazole buffer, in spite of the preservation of folded conformation (in response to IR-exposure, Fig. 8) BSA exhibits higher tendency to adsorb and aggregate than the protein in its denaturated state deposited from non-irradiated solution. To explain these phenomena additional interfacial characteristics have to be invoked. For proteins like BSA and OVA, with significantly larger surface hydrophobicity than that of Lys (Table 1), their water affinity increases in the presence of surface active species due to reduced protein-water interfacial tension when adsorbed ions interact with water molecules [43,45]. Our results suggest that, in the absence of structural change, displacement of those surface-adsorbed ions can be responsible for effective reduction of hydrophilicity of the IR-exposed proteins. The plausible mechanism underlying such effect of IR light stands from the ability of weak electromagnetic radiations to induce motion of nanobubbles in solution and promote

bubble to bubble and bubble to border attraction as it was described in a series of previous studies [73-75]. When bubbles migrate to the surface they can attach to non-polar compartments of the protein and thus displace surface-adsorbed ions. Because of the intrinsic characteristics of IR light, electromagnetic radiation in this particular range can possibly also induce bubble nucleation due to local heating effect (near protein surface) resulting in spots of reduced gas solubility [76]. It might be interesting at this point to note that supersaturation of gases dissolved in water is not a requirement for the nucleation of surface nanobubbles and the process is strong function of temperature and gas concentration [77,78]. For water in equilibrium with air, nucleation window of air gas bubbles lies in the temperature range from 30˚C to 45˚C [78]. Apart from increasing protein-water interfacial tension (due to ion desorption), nanobubbles are recognized to promote hydrophobic interactions by capillary bridging [79] and have been suggested to specifically drive primary protein fold by inducing mutual attraction of non-polar residues [80]. Bubble-induced displacement of surface active species could, therefore, account for the observed increased tendency of proteins with higher hydrophobic solvent-exposed surface area to aggregate in response to IR-light (Fig. 3) and to partition more effectively to the solid. (Fig. 5). Apart from that, this can also be a mechanism supporting native protein fold as the strength of potentially denaturating protein-solvent interactions (supported by adsorbed species) is reduced. IR-induced movement of bubbles (which tend to accumulate at hydrophobic, but escape from the vicinity of hydrophilic surfaces) may well be responsible for the observed hydration enhancement of polar residues. Bubble escape promotes water internal self-structuring (when structure-distorting cavities are removed), what is expressed e.g. in increased surface tension of water [74]. The

proposed explanation is also corroborated by our experimental preliminary observation that IR light has no impact on degassed protein solutions (Fig. S1 Supplementary material) that will be the subject of the forthcoming paper. The latter is in agreement with previous studies showing that effects of weak electromagnetic radiations vanish in solutions devoid of gasses [73-75, 81].

4. Summary and Conclusions

Our results imply that the remote physical trigger – the infrared light – can modify protein structural conformation and protein interfacial characteristics. These factors define protein-water affinity, the feature that modulates protein propensity to partition to the surface. Thanks to these effects, IR light modulates protein adhesion (e.g. protein corona formation) and cohesion (e.g. aggregation of protein-coated nanoparticles) behaviour. Furthermore, IR-induced protection from denaturation on the adsorption process suggests that IR-exposed proteins can possibly maintain their intrinsic activity while immobilized on the solid surface. Further to this end, it has also been recognized that increased protein conformational stability protects the latter from irreversible adsorption [57,82] and that IR-light prevents protein from non-specific aggregation in solution [23]. These phenomena can have important implications for bioengineering applications and for deeper understanding of the effect of electromagnetic radiation on protein physiological functionality. In the latter context, it has been shown for example that previous exposure to IR light protects skin cells from adverse effects of UV radiation [83]. Our results suggest that protective action of IR radiation on protein conformation is

related with the effect of IR light on protein interfacial water and the presence of strongly water-holding amino acid residues.

Competing interest

Authors declare no competing interests

Acknowledgments

This work was financially supported by National Science Centre through grant FUGA number DEC-2015/16/S/ST4/00465.

References

[1] I. Lynch, K. A. Dawson, Protein-nanoparticle interactions, Nanotoday 3 (2008) 40-47.

[2] A.E. Nel, L. Mädler, D. Velegol, T. Xia, E.M.V Hoek, P. Somasundaran, F. Klaessig, V. Castranova, M. Thompson, Understanding biophysicochemical interactions at the nano-bio interface, Nature Materials 8 (2009) 543-557.

[3] F. Turci, E. Ghibaudi, M. Colonna, B. Boscolo, I. Fenoglio, B. Fubini, An integrated approach to the study of the interaction between proteins and nanoparticles, Langmuir 26, (2010) 8336-8346.

[4] A.E. Larsen, D.G. Grier, Like-charge attractions in metastable colloidal crystallites, Nature 385 (1997) 230-233.

[5] T. E. Angelini, H. Liang, W. Wriggers, G.C.L. Wong, Like-charge attraction between polyelectrolytes induced by counterion charge density waves, Proc. Natl. Acad. Sci. USA 100 (2003) 8634-8637.

[6] R. Zhang, B.I. Shklovskii, Long-range polarization attraction between two different like-charged macroions, Phys. Rev. E 72 (2005) 021405

[7] E. Nagornyak, H. Yoo, G.H. Pollack, Mechanism of attraction between like-charged particles in aqueous solution, Soft Matter 5 (2009) 3850-3857.

[8] J. Lekner, Electrostatics of two charged conducting spheres, Proc. A, R. Soc. 468, (2012) 2829-2848.

[9] W. Li, B.A. Persson, M. Morin, M.A. Behrens, M. Lund, M.Z. Oskolkova, Charge-induced patchy attractions between proteins, J. Phys. Chem. B 119 (2015) 503-508.

[10] M. Lund, Anisotropic protein–protein interactions due to ion binding, Colloids and Surfaces B: Biointerfaces 137 (2016) 17-21.

[11] W. Kung, P. Gonzalez-Mozuelos, M. Olvera de la Cruz, A minimal model of nanoparticle crystallization in polar solvents via steric effects, J. Chem. Phys. **133**, (2010) 074704-074709.

[12] W. Kung, P. Gonzalez-Mozuelos, M. Olvera de la Cruz, Nanoparticles in aqueous media: crystallization and solvation charge asymmetry, Soft Matter 6 (2010) 331-341.

[13] M. Ahmad, W. Gu, T. Geyer, V. Helms, Adhesive water networks facilitate binding of protein interfaces, Nat. Commun. 2 (2011) 261.

[14] C.N. Nanev, Brittleness of protein crystals, Cryst. Res. Technol. 47 (2012) 922-927.

[15] J.N. Israelashvili, Intermolecular and Surface Forces, 3rd Ed, Elsevier 2011

[16] M. Heyden, M. Havenith, Combining THz spectroscopy and MD simulations to study protein-hydration coupling, Methods 52, (2010) 74-83.

[17] S. Combet, J.-M. Zanotti, Further evidence that interfacial water is the main "driving force" of protein dynamics: a neutron scattering study on perdeuterated C-phycocyanin, Phys. Chem. Chem. Phys. 14 (2012) 4927-4934.

[18] H. Yoo, E. Nagornyak, R. Das, A.D. Wexler, G.H. Pollack, Contraction-induced changes in hydrogen bonding of muscle hydration water, J. Phys. Chem. Lett. 5 (2014) 947-952.

[19] G. Schiro, Y. Fichou, F.–X. Gallat, K. Wood, F. Gabel, M. Moulin, M. Hartlein, M. Heyden, J.-P. Colletier, A. Orecchini, A. Paciaroni, J. Wuttke, D.J. Tobias, M. Weik, Translational diffusion of hydration water correlates with functional motions in folded and intrinsically disordered proteins, Nat. Commun. 6, (2015), 6490.

[20] J. Dielmann-Gessner, M. Grossman, V. Conti Nibali, B. Born, I. Solomonov, G.B. Fields, M. Havenith, I. Sagi, Enzymatic turnover of macromolecules generates long-lasting protein-water-coupled motions beyond reaction steady state, Proc. Natl. Acad. Sci. USA 111 (2014) 17857-17862.

[21] M.-C. Bellissent-Funel, A. Hassanali, M. Havenith, R. Henchman, P. Pohl, F. Sterpone, D. van der Spoel, Y. Xu, A.E. Garcia, Water determines the structure and dynamics of proteins, Chem. Rev. 116 (2016) 7673-7697.

[22] J. Zheng, W.-C. Chin, E. Khijniak, E. Khijniak Jr, G.H. Pollack, Surfaces and interfacial water: evidence that hydrophilic surfaces have long-range impact, Adv. Colloid Interface Sci. 127 (2006) 19-27.

[23] M. Kowacz, M. Marchel, L. Juknaité, J.M.S.S. Esperanca, M.J. Romao, A.L. Carvalho, L.P.N. Rebelo, Infrared light-induced protein crystallization. Structuring of protein interfacial water and periodic self-assembly, J. Crystal Growth 457 (2017) 362-368.

[24] Q. Zhao, J. Zheng, B. Chai, G.H. Pollack, Unexpected effect of light on colloidal crystal spacing, Langmuir 24 (2008) 1750-1755.

[25] E.I. Vargha-Butler, S. Sveinsson, Z. Policova, Wettability studies on drugs and drug delivery vesicles, September 1991Colloids and Surfaces 58 (1991) 271-286.

[26] The Imaging Source, IC Measure. https://www.theimagingsource.com/products/software/end-user-software/ic-measure/, 2016 (accessed 4 December 2017).

[27] B. Chai, H. Yoo, G. H. Pollack, Effect of radiant energy on near-surface water, J. Phys. Chem. B 113 (2009) 13953–13958.

[28] D. W. Lee, X. Banquy, K. Kristiansen, Y. Min, A. Ramachandran, J.M. Boggs, J.N. Israelachvili, Adsorption mechanism of myelin basic protein on model substrates and its bridging interaction between the two surfaces, Langmuir 31 (2015) 3159-3166.

[29] G. Sauerbrey, The use of oscillators for weighing thin layer and for microweighing, J. Phys. 155 (1959) 206-212.

[30] M.E. Goldberg, A.F. Chaffotte, Undistorted structural analysis of soluble proteins by attenuated total reflectance infrared spectroscopy, Protein Sci. 14 (2005) 2781-2792.

[31] H. Yang, S. Yang, J. Kong, A. Dong, S. Yu, Obtaining information about protein secondary structures in aqueous solution using Fourier transform IR spectroscopy, Nature Prot. 10 (2015) 382-396.

[32] C. Pfeiffer, C. Rehbock, D. Huhn, C. Carrillo-Carrion, D. J. de Aberasturi, V. Merk, S. Barcikowski, W. J. Parak , Interaction of colloidal nanoparticles with their local environment: the (ionic) nanoenvironment around nanoparticles is different from bulk and determines the physico-chemical properties of the nanoparticles, J. R. Soc. Interface 11 (2014) 20130931.

[33] M. Barisik, S. Atalay, A. Beskok, S. Qian, Size dependent surface charge properties of silica nanoparticles, J. Phys. Chem. C 118 (2014) 1836–1842.

[34] U.K. Aravind, J. Mathew, C.T. Aravindakumar, Transport studies of BSA, lysozyme and ovalbumin through chitosan/polystyrene sulfonate multilayer membrane, Membrane Sci. 299 (2007) 146-155.

[35] M. Cardamone, N. K. Puri, Spectrofluorimetric assessment of the surface hydrophobicity of proteins, Biochem. J. 282 (1992) 589-593.

[36] M. Ries-Kautt, A. Ducruix, Crystallization of previously desalted lysozyme in the presence of sulfate ions, Acta Cryst. D 50 (1994) 366-369.

[37] M. Brunsteiner, M. Flock, B. Nidetzky, Structure based descriptors for the estimation of colloidal interactions and protein aggregation propensities, PLOS ONE 8 (2013) e59797.

[38] G.R. Tristam, Amino acid composition of the proteins, in H. Neurath, K. Bailly (Eds), The Proteins, New York Academic Press Inc., New York 1, Part A, 1953, pp. 181-233.

[39] L. Vrbka, P. Jungwirth, P. Bauduin, D. Touraud, W. Kunz, Specific ion effects at protein surfaces: A molecular dynamics study of bovine pancreatic trypsin inhibitor and horseradish peroxidase in selected salt solutions, J. Phys. Chem. B 110 (2006) 7036-7043.

[40] B. Minofar, P. Jungwirth, M.R. Das, W. Kunz, S. Mahiuddin, Propensity of formate, acetate, benzoate, and phenolate for the aqueous solution/vapor interface: Surface tension measurements and molecular dynamics simulations, J. Phys. Chem. C 111 (2007) 8242-8247.

[41] B. Minofar, R. Vácha, A. Wahab, S. Mahiuddin, W. Kunz, P. Jungwirth, Propensity for the air/water interface and ion pairing in magnesium acetate vs magnesium nitrate solutions: Molecular dynamics simulations and surface tension measurements, J. Phys. Chem. B 110 (2006) 15939-15944.

[42] P. Jungwirth, Spiers memorial lecture. Ions at aqueous interfaces, Faraday Discussions 141 (2009) 9-30.

[43] J. Paterová, K. B. Rembert, J. Heyda, Y. Kurra, H. I. Okur, W. R. Liu, C. Hilty, P. S. Cremer, P. Jungwirth, Reversal of the Hofmeister Series: Specific ion effects on peptides, J. Phys. Chem. B 117 (2013) 8150-8158.

[44] M. Lund, L. Vrbka, P. Jungwirth, Specific ion binding to nonpolar surface patches of proteins, J. Am. Chem. Soc. 130 (2008) 11582–11583.

[45] Y. Zhang, P.S. Cremer, The inverse and direct Hofmeister series for lysozyme, Proc. Natl. Acad. Sci. U S A. 106 (2009) 15249-15253.

[46] M. Lund, P. Jungwirth, C.E. Woodward, Ion specific protein assembly and hydrophobic surface forces, Phys. Rev. Lett. **100** (2008) 258105.

[47] Y.R. Gokarn, R. M. Fesinmeyer, A. Saluja, V. Razinkov, S.F. Chase, T.M. Laue, D.N. Brems, Effective charge measurements reveal selective and preferential accumulation of anions, but not cations, at the protein surface in dilute salt solutions. Protein Sci. 20 (2011) 580-587.

[48] M. Kowacz, A. Mukhopadhyay, A.L. Carvalho, J.M.S.S. Esperança, M.J. Romão, L.P.N. Rebelo, Hofmeister effects of ionic liquids in protein crystallization: Direct and water-mediated interactions, CrystEngComm 14 (2012) 4912-4921.

[49] D. Bastos-Gonzaleza, L. Pérez-Fuentesa, C. Drummond, J. Faraudo, Ions at interfaces: the central role of hydration and hydrophobicity, Curr. Opinion in Colloid Interface Sci. 23 (2016) 19-28.

[50] S. Salgin, U. Salgin, S. Bahadir, Zeta potentials and isoelectric points of biomolecules: The effects of ion types and ionic strengths, Int. J. Electrochem. Sci. 7 (2012) 12404 – 12414.

[51] Y. R. Dahal, J. D. Schmit, Ion specificity and nonmonotonic protein solubility from salt entropy, Biophysical J. 114 (2018) 76-87.

[52] H. Sigel, R. Tribolet, O. Yamauchi, The imidazole group and its stacking properties in mixed ligand metal ion complexes, J. Critical Discussion Curr. Lit. 9 (1990) 305-330.

[53] U. Domanska, M.K. Kozlowska, J. Chem. Eng. Data 47 (2002) 456-466.

[54] C.A. Haskard, E.C.Y. Li-Chan, Hydrophobicity of bovine serum albumin and ovalbumin determined using uncharged (PRODAN) and anionic (ANS-) fluorescent probes, J. Agric. Food Chem. 46 (1998) 2671-2677.

[55] M.F. Cuddy, A.R. Poda, L.N. Brantley, Determination of isoelectric points and the role of pH for common quartz crystal microbalance sensors, Appl. Mater. Interfaces 5 (2013) 3514-3518.

[56] Z. Adamczyk, M.Nattich, M.Wasilewska, M.Zaucha, Colloid particle and protein deposition — Electrokinetic studies, adv. Colloid interf. Sci 168 (2011) 3-28.

[57] C. Mathé, S. Devineau, J.-C. Aude, G. Lagniel, S. Chédin, V. Legros, M.-H. Mathon, J.-P. Renault, S. Pin, Y. Boulard, J. Labarre, Structural determinants for protein adsorption/non-adsorption to silica surface**,** PLoS ONE 8 (2013) e81346.

[58] C.M. Alves, R.L. Reis, J.A. Hunt, The competitive adsorption of human proteins onto natural-based biomaterials, J. R. Soc. Interface **7** (2010) 1367-1377.

[59] M. Kowacz, M. Marchel, J.M.S.S. Esperança, L.P.N. Rebelo, Ionic liquid-functionalized crystals of barium sulfate: A hybrid organic–inorganic material with tuned hydrophilicity and solid–liquid behavior, Materials Chem. Phys. 160 (2015) 308-314.

[60] M. Wlodek, M. Szuwarzynski, M. Kolasinska-Sojka, Effect of supporting polyelectrolyte multilayers and deposition conditions on the formation of 1‑palmitoyl-2-oleoyl-sn-glycero-3-phosphocholine/1-palmitoyl-2-oleoyl-sn-glycero-3-phosphoethanolamine lipid bilayers, Langmuir 31 (2015) 10484−10492.

[61] K. Murayama, M. Tomida, Heat-induced secondary structure and conformation change of bovine serum albumin investigated by Fourier transform infrared spectroscopy**,** Biochemistry 43 (2004) 11526-11532.

[62] R.S. Vieira-Pires, J.H. Morais-Cabral, 3_{10} helices in channels and other membrane proteins, J. General Physiology 136 (2010) 585-592.

[63] M. Bellanda, S. Mammi, S. Geremia, N. Demitri, L. Randaccio, Q.B. Broxterman, B. Kaptein, P. Pengo, L. Pasquato, P. Scrimin, Solvent polarity controls the helical conformation of short peptides rich in C alpha-tetrasubstituted amino acids, Chem. Eur. J. 13 (2007) 407-416.

[64] M.E. Karpen, P. de Haseth, K.E. Neet, Differences in the amino acid distributions of 3(10)-helices and alpha-helices, Protein Sci. 1 (1992) 133-1342.

[65] H.Y. Hu, H.N. Du, Alpha-to-beta structural transformation of ovalbumin: heat and pH effects**,** J. Protein Chem. 19 (2000) 177-183.

[66] K.V. Abrosimova, O.V. Shulenina, S.V. Paston, FTIR study of secondary structure of bovine serum albumin and ovalbumin, J. Physics: Conference Series 769 (2016) 012016.

[67] L. Lins, A. Thomas, R. Brasseur, Analysis of accessible surface of residues in proteins, Prot. Sci. 12 (2003) 1406-1417.

[68] S. Bandyopadhyay, S. Chakraborty, B. Bagchi, Secondary structure sensitivity of hydrogen bond lifetime dynamics in the protein hydration layer, J. Am. Cem. Soc. 127 (2005)16660-16667.

[69] M.R. Panman, B.H. Bakker, D. den Uyl, E.R. Kay, D.A. Leigh, W.J. Buma, A.M. Brouwer, J.A.J. Geenevasen, S. Woutersen, Water lubricates hydrogen-bonded molecular machines, Nature Chem. 5 (2013) 929-934.

[70] J. Hou, D.H. Veeregowda, J. De Vries, H.C. Van der Mei, H.J. Busscher, Structured free-water clusters near lubricating surfaces are essential in water-based lubrication, J. R. Soc. Interface 13 (2016) 20160554.

[71] S. Mitaku, T. Hirokawa, T. Tsuji, Amphiphilicity index of polar amino acids as an aid in the characterization of amino acid preference at membrane-water interfaces, Bioinformatics 18 (2002) 608-616.

[72] L. Lins, A. Thomas, R. Brasseur, Analysis of accessible surface of residues in proteins, Prot. Sci. 12 (2003) 1406-1417

[73] V.M. Shatalov, Mechanism of the biological impact of weak electromagnetic fields and the in vitro effects of blood degassing, Biophysics 57 (2012) 808-813.

[74] V.M. Shatalov, A.E. Filippov, I.V. Noga, Bubbles induced fluctuations of some properties of aqueous solutions, Biophysics 57 (2012) 421-427.

[75] V.M. Shatalov, I.V. Noga, A. Zinchenko, Degassing of bioliquids in low electromagnetic fields, Electronic J. Biol. 6 (2010) 67-72.

[76] S. Deguchi, S. Takahashi, S. Tanimura, H. Hiraki, Producing single microbubbles with controlled size using microfiber, Adv. Biosci. Biotechnol. 2 (2011) 385-390.

[77] C.-K. Fang, H.-C. Ko, C.-W. Yang, Y.-H. Lu, I.-S. Hwang, Nucleation processes of nanobubbles at a solid/water interface, Sci. Reports 6 (2016) 24651.

[78] J.R.T. Seddon, E.S. Kooij, B. Poelsema, H.J.W. Zandvliet, D. Lohse, Surface bubble nucleation stability, Phys. Rev. Lett. 106 (2011) 056101.

[79] M.A. Hampton, A.V. Nguyen, Nanobubbles and the nanobubble bridging capillary force, Adv. Colloid Interface Sci. 154 (2010) 30-35.

[80] S. Sen, H.P. Voorheis, Protein folding: understanding the role of water and the low Reynolds number environment as the peptide chain emerges from the ribosome and folds**,** J. Theor. Biol. 363 (2014) 169-187.

[81] P. Vallée, J. Lafait, L. Legrand, P. Mentré, M. O. Monod, Y. Thomas, Effects of pulsed low-frequency electromagnetic fields on water characterized by light scattering techniques: role of bubbles, Langmuir 21 (2005) 2293-2299.

[82] M. Karlsson, J. Ekeroth, H. Elwing, U. Carlsson, Reduction of irreversible protein adsorption on solid surfaces by protein engineering for increased stability**,** J. Biol. Chem. 280 (2005) 25558-25564.

[83] D. Barolet, F. Christiaens, M.R. Hamblin, Infrared and skin: Friend or foe, J. Photochem. Photobiol. B: Biol. 155 (2016) 78-85.

Figure captions

Fig. 1. Change in sediment volume (in %) of the protein-coated SiO_2 nanoparticles in different (texture coded) environments: water, 20 mM NaCl and 20 mM imidazole buffer (pH = 7.36) with respect to volume of the non-coated solids. Protein coatings correspond to lysozyme (Lys), ovalbumin (OVA) and bovine serum albumin (BSA)

Fig. 2. Hydrodynamic diameter and zeta potential (ZP) of protein (lysozyme (Lys), ovalbumin (OVA) and bovine serum albumin (BSA))-coated SiO_2 nanoparticles dispersed in water. Vertical line shows average size of aggregates of bare SiO_2 dispersed in water (diameter of individual dry SiO_2 particles is about 10-20 nm). OVA and OVA+IR indicate size of the nanoparticles coated with non-irradiated and IR-exposed protein, respectively. For large aggregates formed by Lys and BSA decorated particles there was no statistical difference between control and irradiated systems

Fig. 3. a) Infrared light-induced changes in sediment volume (in %) of the protein-coated SiO_2 nanoparticles in different environments: water, 20 mM NaCl and 20 mM imidazole buffer (pH = 7.36). b) Representative image of the IR-induced changes in sediment volume of protein-coated SiO_2 nanoparticles in imidazole buffer. Each pair of cuvettes presents control (on the left) and irradiated (on the right) conditions; from left to right for Lysozyme (Lys), ovalbumin (OVA) and bovine serum albumin (BSA).

Fig. 4. Frequency (Δf) shifts on adsorption of lysozyme (a), bovine serum albumin (b) and ovalbumin (c) on SiO_2 surface (protein conc. 1mg/ml in Milli-Q water without supporting electrolyte). Grey lines correspond to control conditions; black lines show adsorption of IR-exposed proteins. Arrows indicate beginning of the washing of the sensor with water. Δf is proportional to the adsorbed mass of a protein together with its hydration water. More negative frequency values indicate more mass adsorbed. Initial sharp frequency minima (as illustrated in more detail on Fig. 6) indicate transient adsorption of larger mass and its consecutive loss due to release of hydration water.

Fig. 5. Frequency (Δf) shifts on adsorption of lysozyme (a), bovine serum albumin (b) and ovalbumin (c) from buffered solution (1 mg/ml of protein in 20 mM imidazole of pH = 7.36) on SiO_2 surface. Grey lines correspond to control conditions; black lines show adsorption of IR-exposed proteins. Arrows indicate beginning of the washing of the sensor with buffer.

Fig. 6. Frequency (Δf) - solid lines, and dissipation energy - dashed lines, shifts on initial stages of adsorption of lysozyme (a), bovine serum albumin (b) and ovalbumin (c) on SiO_2 surface. Grey lines indicate control conditions, black lines indicate adsorption of IR-exposed proteins. All proteins at concentration of 1 mg/ml dissolved in Milli-Q water (without supporting electrolyte). Dissipation energy is indicative of viscoelastic properties of the adsorbed film and increasing dissipation means higher softness of the film.

Fig. 7. Fourier deconvoluted and curve-fitted IR spectra of amide I region (1700-1600 cm^{-1}) of BSA in water (left panel) for a) dissolved, b) adsorbed protein and c) protein adsorbed after IR-exposure. Right panel presents respective spectra of BSA in 20 mM NaCl for d) dissolved, e) adsorbed protein and f) protein adsorbed after irradiation. Vertical lines indicate position of peaks corresponding to α-helix conformation in dissolved state. Y-axis corresponds to absorbance in arbitrary units.

Fig. 8. Fourier deconvoluted and curve-fitted IR spectra of amide I region (1700-1600 cm^{-1}) of BSA in 20 mM imidazole buffer (pH = 7.36) for a) dissolved, b) adsorbed protein and c) protein adsorbed after IR-exposure. Vertical lines indicate position of peaks corresponding to α-helix conformation in dissolved state.

Fig. 9 Fourier deconvoluted and curve-fitted IR spectra of amide I region (1700-1600 cm^{-1}) of Lys (a-c) and OVA (d-f) in 20 mM imidazole buffer (pH = 7.36). Left panel presents respective spectra of Lys for a) dissolved, b) adsorbed protein and c) protein adsorbed after IR-exposure. Right panel presents spectra pof OVA for d) dissolved, e) adsorbed protein and f) protein adsorbed after irradiation. Vertical lines indicate position of peaks corresponding to α-helix conformation in dissolved state.

Figure 1.

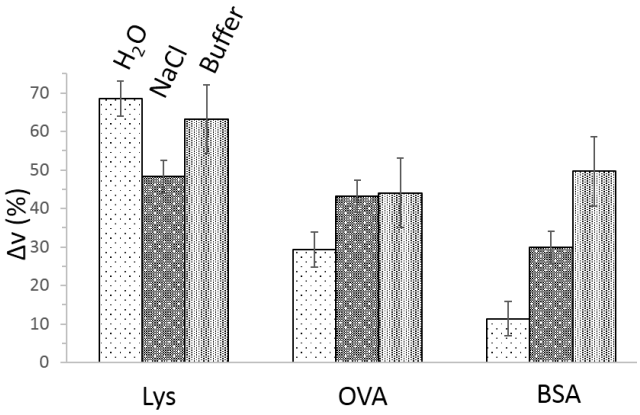

Figure 2.

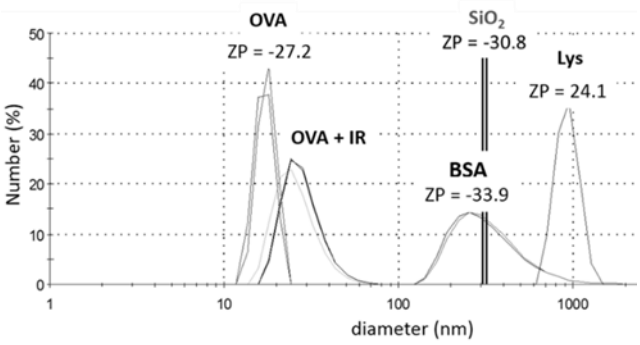

Figure 3.

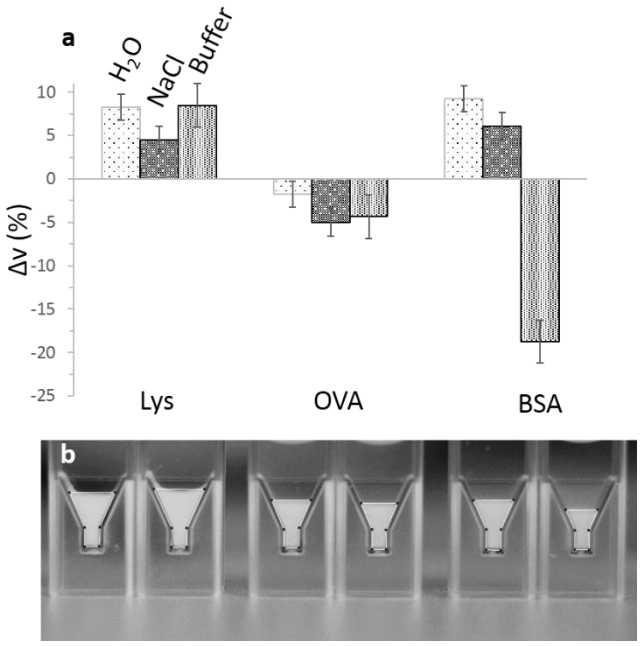

Figure 4.

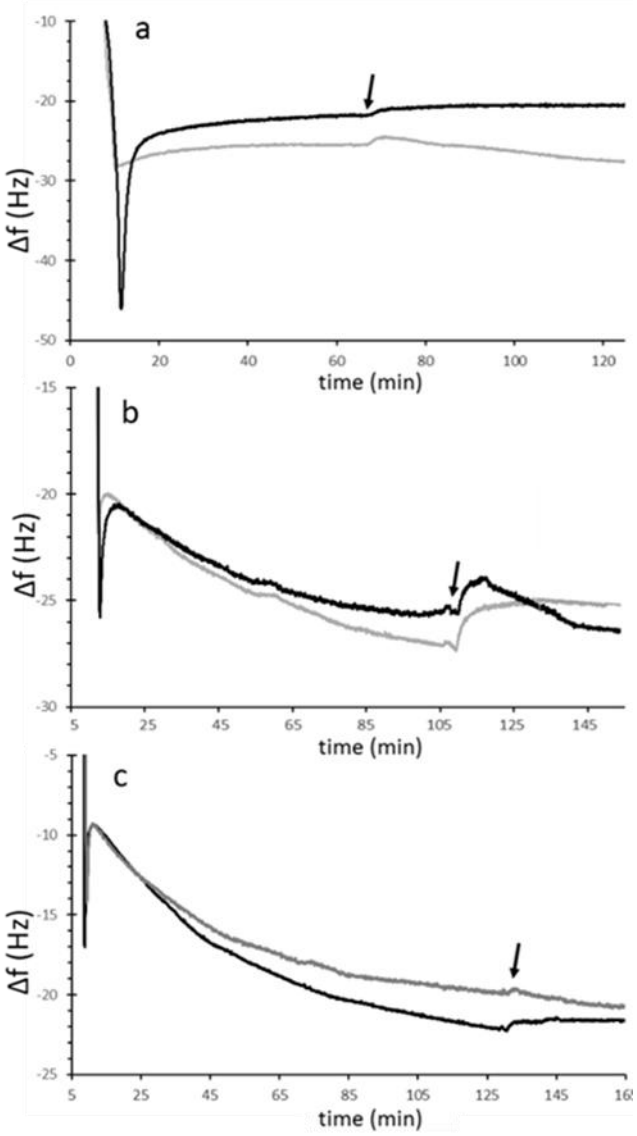

Figure 5.

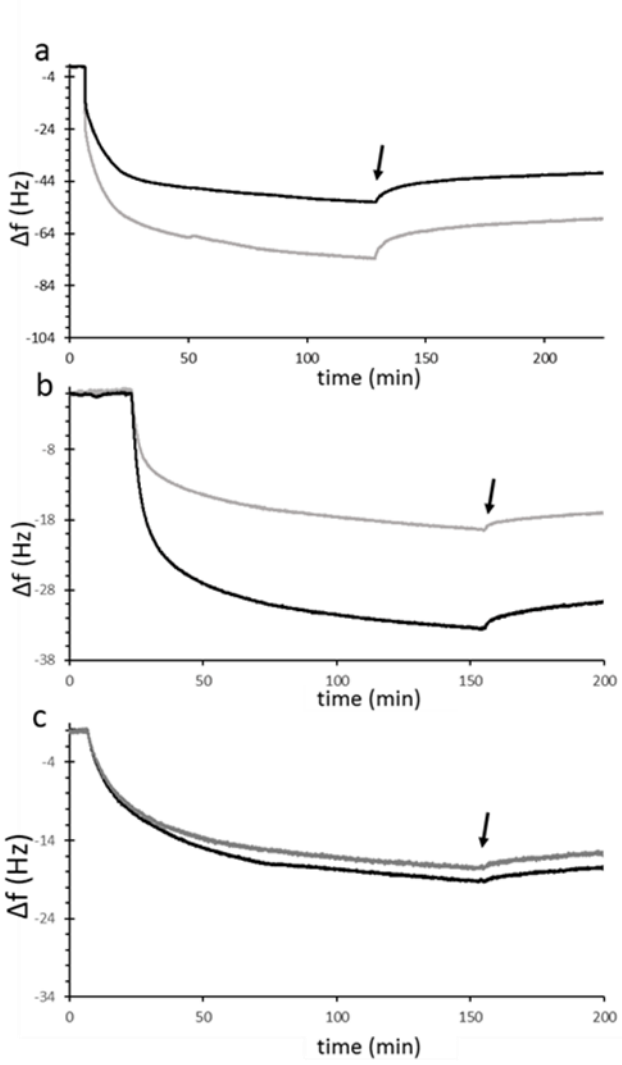
a
-4
-24
-44
-64
-84
-104
Δf (Hz)
0
50
100
150
200
time (min)
b
-8
-18
-28
-38
Δf (Hz)
0
50
100
150
200
time (min)
c
-4
-14
-24
-34
Δf (Hz)
0
50
100
150
200
time (min)

Figure 6.

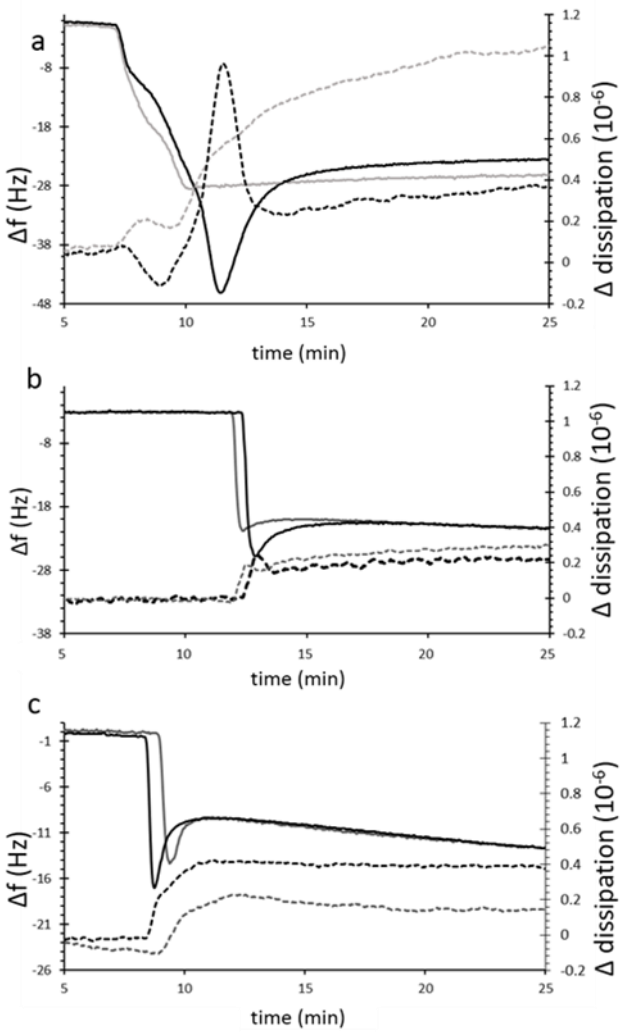

Figure 7.

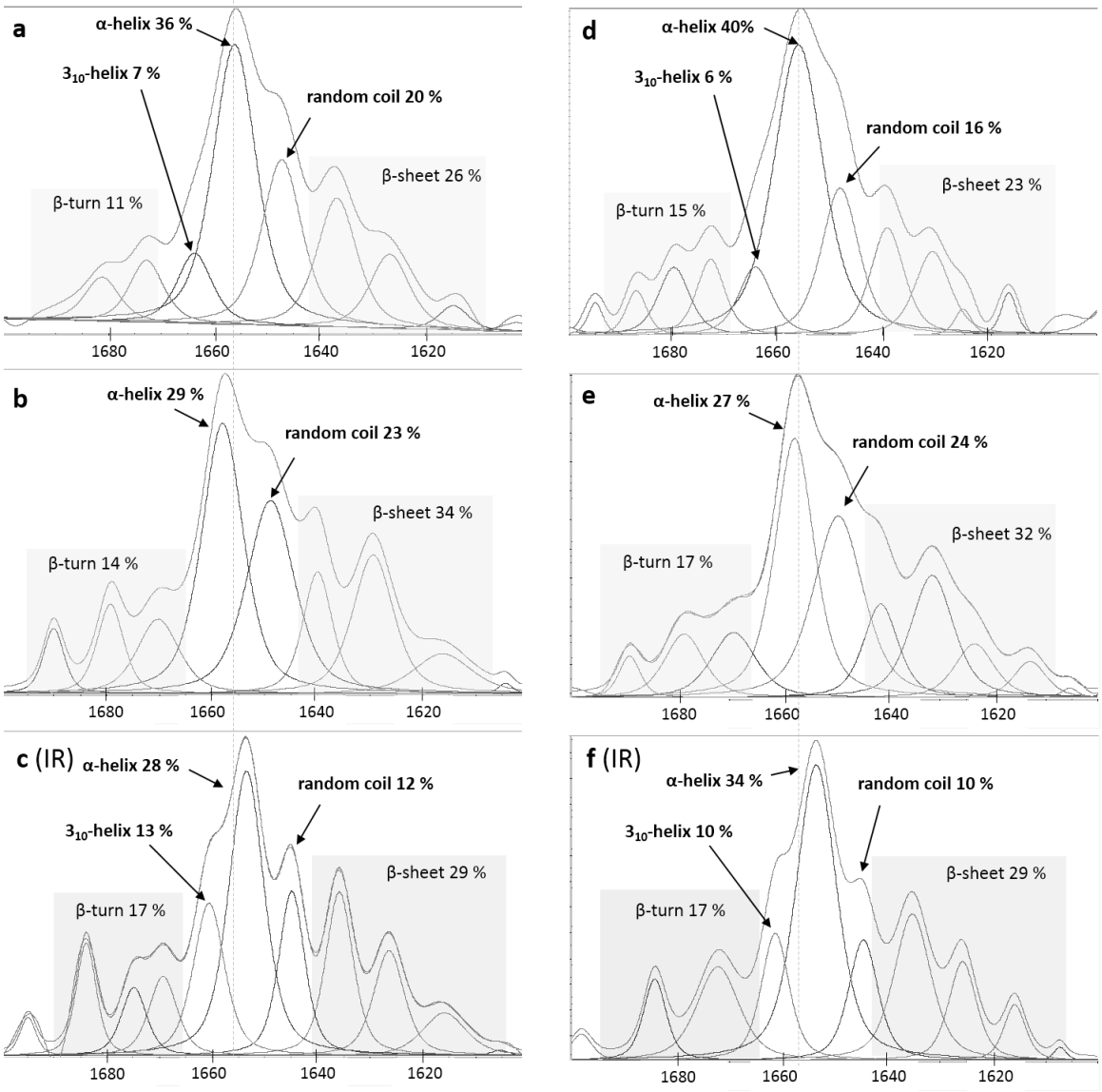
a
α-helix 36 %
3$_{10}$-helix 7 %
random coil 20 %
β-sheet 26 %
β-turn 11 %
d
α-helix 40%
3$_{10}$-helix 6 %
random coil 16 %
β-sheet 23 %
β-turn 15 %
b
α-helix 29 %
random coil 23 %
β-sheet 34 %
β-turn 14 %
e
α-helix 27 %
random coil 24 %
β-sheet 32 %
β-turn 17 %
c (IR)
α-helix 28 %
3$_{10}$-helix 13 %
random coil 12 %
β-sheet 29 %
β-turn 17 %
f (IR)
α-helix 34 %
3$_{10}$-helix 10 %
random coil 10 %
β-sheet 29 %
β-turn 17 %
1680
1660
1640
1620
Wavenumber (cm^{-1})

Figure 8.

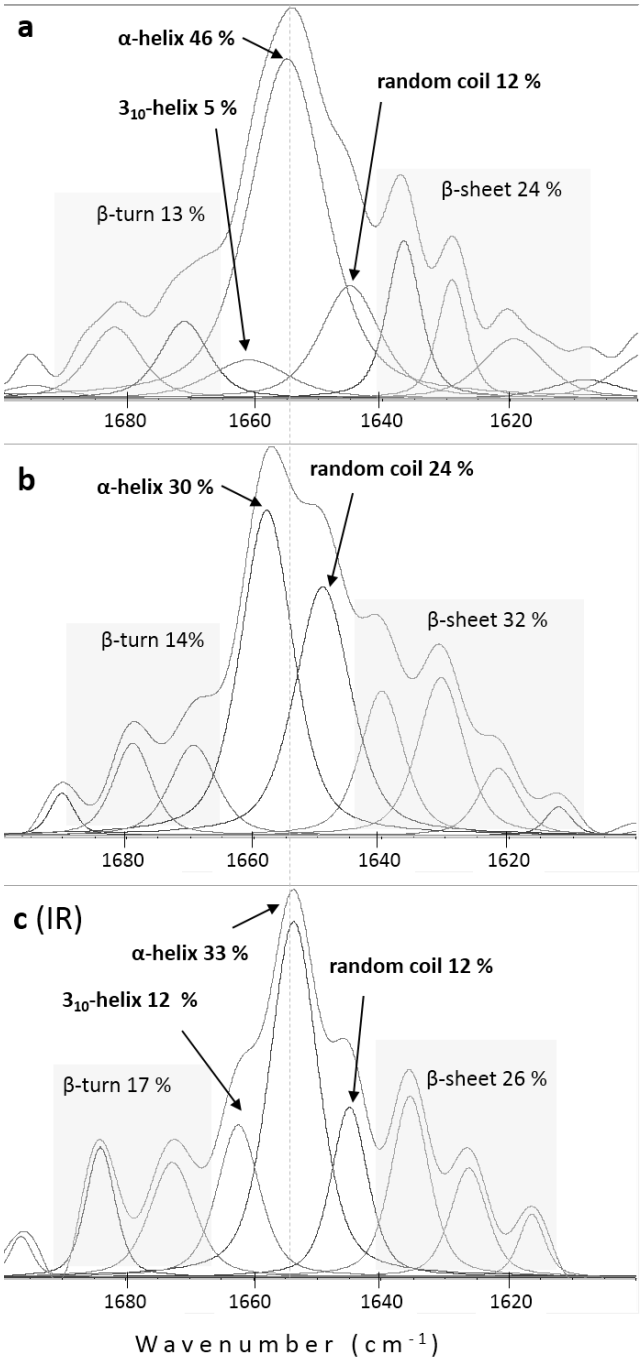
a
α-helix 46 %
3$_{10}$-helix 5 %
random coil 12 %
β-turn 13 %
β-sheet 24 %
1680
1660
1640
1620
b
α-helix 30 %
random coil 24 %
β-turn 14%
β-sheet 32 %
1680
1660
1640
1620
c (IR)
α-helix 33 %
3$_{10}$-helix 12 %
random coil 12 %
β-turn 17 %
β-sheet 26 %
1680
1660
1640
1620
Wavenumber (cm^{-1})

Figure 9.

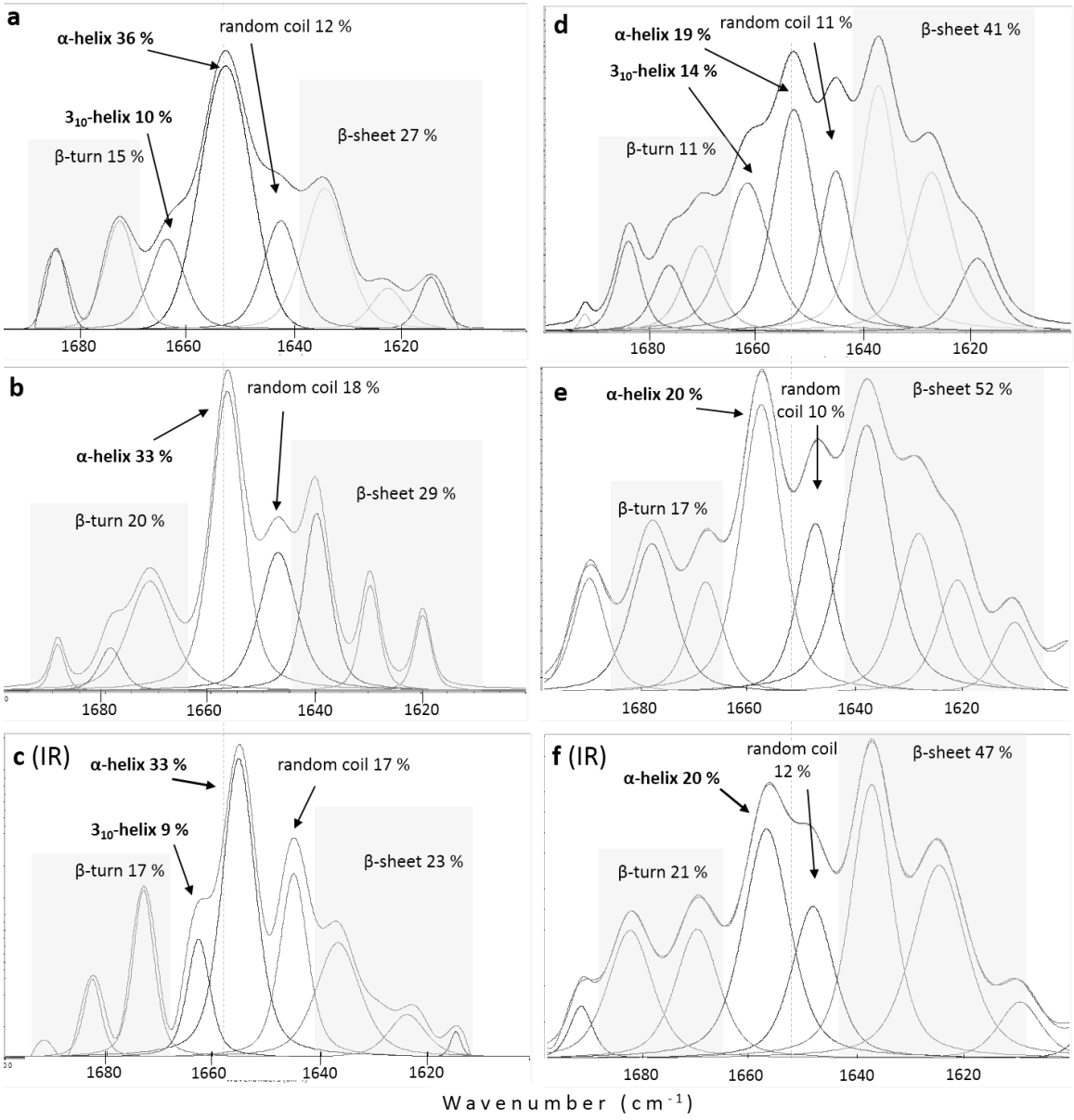
a
α-helix 36 %
random coil 12 %
3₁₀-helix 10 %
β-turn 15 %
β-sheet 27 %
1680
1660
1640
1620
d
α-helix 19 %
random coil 11 %
β-sheet 41 %
3₁₀-helix 14 %
β-turn 11 %
1680
1660
1640
1620
b
random coil 18 %
α-helix 33 %
β-sheet 29 %
β-turn 20 %
1680
1660
1640
1620
e
α-helix 20 %
random
coil 10 %
β-sheet 52 %
β-turn 17 %
1680
1660
1640
1620
c (IR)
α-helix 33 %
random coil 17 %
3₁₀-helix 9 %
β-turn 17 %
β-sheet 23 %
1680
1660
1640
1620
f (IR)
random coil
12 %
α-helix 20 %
β-sheet 47 %
β-turn 21 %
1680
1660
1640
1620
Wavenumber (cm⁻¹)

Supplementary Information

Effect of infrared light on protein behavior in contact with solid surfaces

Magdalena Kowacz[*] *and Piotr Warszyński*

Jerzy Haber Institute of Catalysis and Surface Chemistry Polish Academy of Sciences; Niezapominajek 8, PL-30239 Krakow

*****Corresponding author: nckowacz@cyf-kr.edu.pl

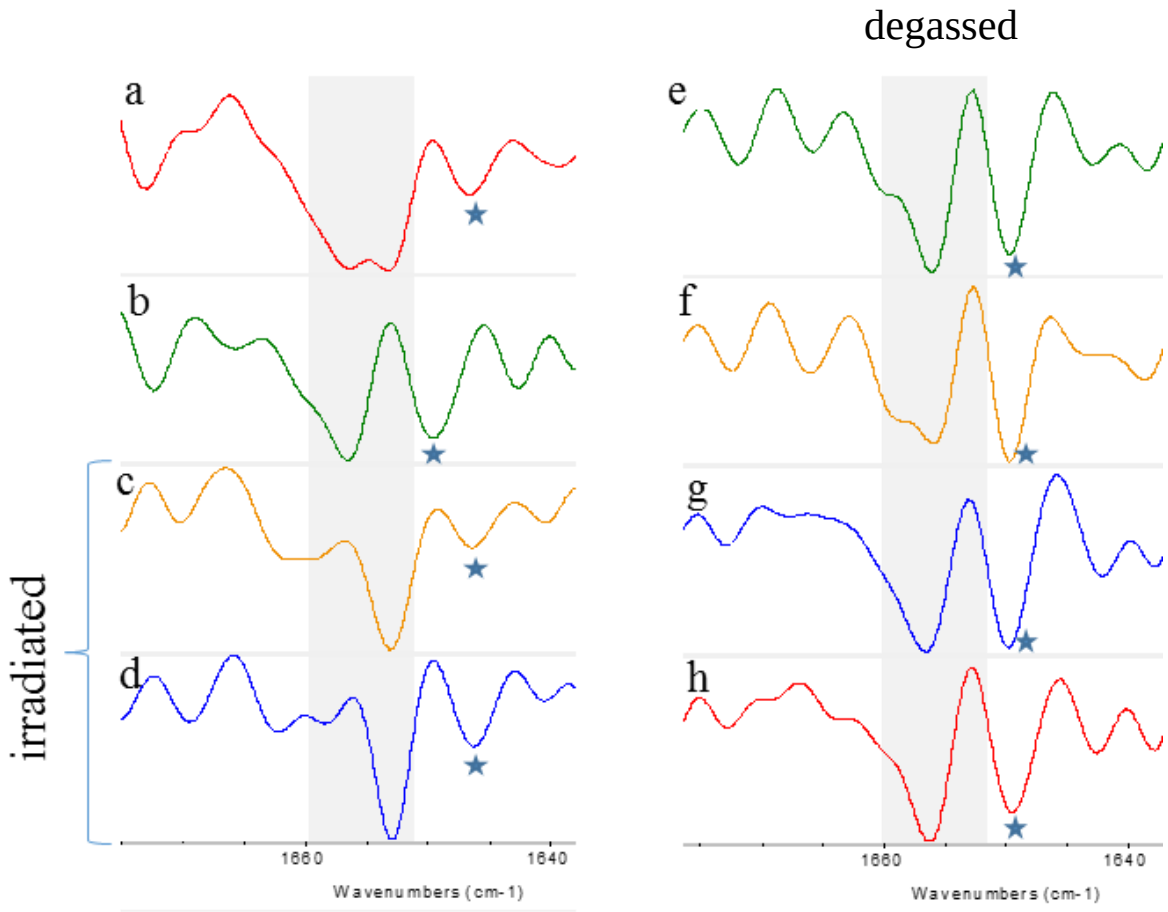

Fig. S1 Second derivative of FTIR-ATR spectra of bovine serum albumin (BSA) deposited from controlled (a-d) and degassed[a] solutions (e-h). Panels a-b and e-f correspond to consecutive spectra of the protein deposited from non-irradiated solutions. Panels c-d and g-h correspond to consecutive spectra of the protein deposited from solutions after IR-exposure[b], in control and degassed system, respectively. Shaded areas indicate region ascribed to helical conformation, stars

mark peaks ascribed to random coil structures. Note that in degassed system (e-h) there is virtually no effect of IR on relative contributions of helical and random structures. In controlled (non-degassed) system (a-d) IR exposure has significant effect on protein conformation and supports preservation of helical fold on the adsorption process.

[a] Degassing was achieved by subjecting protein solution to vacuum pumping at pressure of 50 mbar for 2 hours.

[b] 250 µl of the BSA solution was irradiated for 10 min with the use of Light Emitting Diode with emission maximum at 2900 nm.